Supplementary Information S2

The role of temperature in the photoluminescence quantum yield (PLQY) of Ag_2S-based nanocrystals

Peijiang Wang,[a] Rafael Morales-Márquez,[a] Gabriel Cervás,[b] Alejandro Hernández Medel,[c,d] Marina Paris Ogayar,[d] D. Jimenez de Aberasturi,[e] Ana Ines de Isidro-Gomez,[c] Almudena Torres-Pardo,[f] Francisco Javier Palomares,[a] Saül Garcia-Orrit,[g] Célia T. Sousa,[c] Ana Espinosa,[a] Helmut H. Telle,[b] Dirk H. Ortgies,[d,h,i,j] Víctor Vega-Mayoral,[g] Juan Cabanillas-González,[g] Emma Martín Rodríguez, [c,d,h,i,j]* Ute Resch-Genger,*[k] K. David Wegner,*[k] and Beatriz H. Juarez.*[a]

[a] *Materials Science Institute of Madrid, ICMM. Spanish Research Council, CSIC, C/ Sor Juana Inés de la Cruz, 3, 28049 Madrid, Spain. Email: bh.juarez@csic.es*
[b] *Departamento de Química Física Aplicada, Facultad de Ciencias, Universidad Autónoma de Madrid, C/ Francisco Tomás y Valiente 7, 28049, Madrid, Spain.*
[c] *Departamento de Física Aplicada, Facultad de Ciencias, Universidad Autónoma de Madrid, C/ Francisco Tomás y Valiente 7, 28049, Madrid, Spain Madrid,*
[d] *Nanomaterials for BioImaging Group (NanoBIG), Facultad de Ciencias, Universidad Autónoma de Madrid, C/ Francisco Tomás y Valiente 7, 28049, Madrid, Spain. Email: emma.martin@uam.es*
[e] *SpainCiCbiomaGUNE, Basque Research and Technology Alliance (BRTA), Miramon Pasealekua, 182, 20014 Donostia-San Sebastián, Gipuzkoa, Spain and Centro de Investigación Biomédica en Red de Bioingeniería, Biomateriales and Nanomedicina (CIBER-BBN), 20014 Donostia-San Sebastián, Spain.Ikerbasque, Basque Foundation for Science, 48009 Bilbao, Spain.*
[f] *Inorganic Chemistry Department, Chemical Sciences Faculty, Universidad Complutense de Madrid, 28040 Madrid, Spain and ICTS National Center for Electronic Microscopy, Universidad Complutense, 28040 Madrid, Spain*
[g] *IMDEA Nanoscience, Faraday 9, Campus de Cantoblanco, 28049 Madrid, Spain.*
[h] *Nanomaterials for BioImaging Group (nanoBIG), Instituto Ramón y Cajal de Investigación Sanitaria (IRYCIS), Ctra. Colmenar Viejo, km. 9,100, 28034 Madrid, Spain. Email: emma.martin@uam.es*
[i] *Institute for Advanced Research in Chemical Sciences (IAdChem), Universidad Autónoma de Madrid, 28049 Madrid, Spain.*
[j] *Instituto de Ciencia de Materiales Nicolás Cabrera, Universidad Autónoma de Madrid, 28049 Madrid, Spain.*
[k] *Bundesanstalt für Materialforschung und -prüfung (BAM), Richard-Willstaetter-Str. 11, 12489Berlin, Germany. Email: karl-david.wegner@bam.de, ute.resch@bam.de*

S2 – Supplementary information related to experimental results

Index

S2.1 – Structural and compositional characterization using TEM and XPS

(A) Transmission Electron Microscopy – TEM

The timing effect of the S injection in the pot

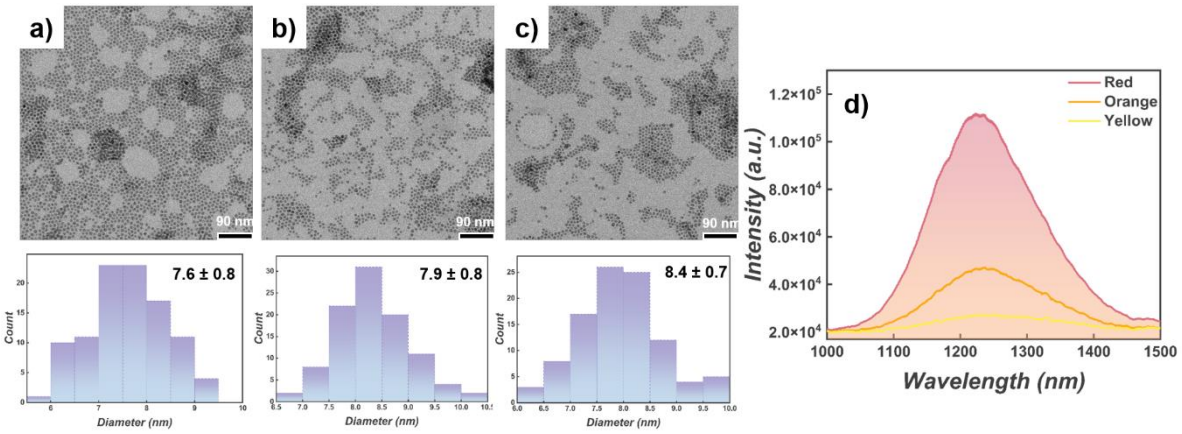

Figure S1: Ag_2S NCs obtained by injecting S@OLA when the Ag-precursor shows (a) yellow, (b) orange or (c) red colours (see main text), and corresponding histograms obtained from the measurements of 100 NCs in each TEM image. d) PL spectra of the NCs solutions (a-c) at the same Ag-concentration. The right moment to inject the S@OLA solution is when the precursor solution just turns red. The PL spectra in this case were acquired with a different detector than the one used for the rest of the PL measurements shown along the manuscript.

High-resolution TEM characterization (HRTEM)

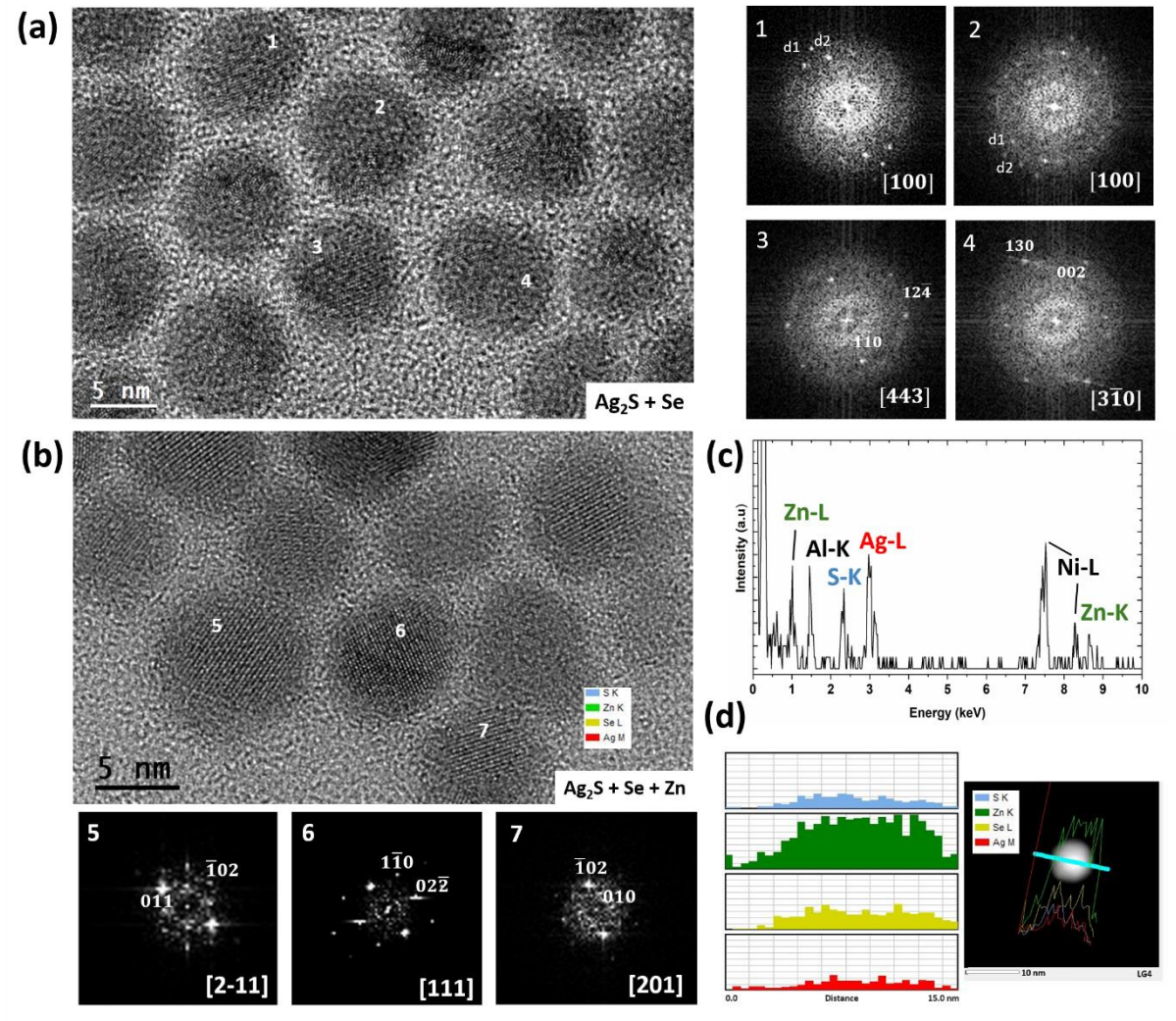

Figure S2: (a) HRTEM characterization of CS NCs, along with FFT indexation of the four NCs labelled 1, 2, 3 and 4. Distances d_1=0.693 nm and d_2=0.735 nm corresponding to (001) and (001) interplanar spacings, respectively, are identified at FFTs from NCs 1 and 2. (b) HRTEM characterization of CSS NCs treated with Zn, with FFT indexation of the three NCs labelled 5, 6 and 7. (c) EDX spectrum and (d) EDX mapping acquired during long exposure times, evidencing the presence of S, Zn, Se and Ag across the volume of the NC, as shown in the image on the right.

(B) X-ray photoelectron spectroscopy – XPS

Evidence of the formation of ZnS and a thicker shell in air

The synthesis of NCs in air or in N_2 atmosphere influences the final PLQY. While the S-injection and the Se-injection do not critically influence the PL response of the NCs, the treatment with the Zn oleate-stock-solution produces higher PLQY values when it is performed in air.

A detailed line shape analysis of XPS core level spectra is required in order to obtain information of Zn, S and Ag distribution along the CSS structures. The spectra of CSS NCs produced in air or in N_2 are dominated by the strong emission from Ag $3d_{5/2}$ peak, at binding energy values of around 368.1 eV, together with its spin-orbit doublet counterpart Ag $3d_{3/2}$, shifted 6.00 eV towards higher binding energy (spectra not shown). In addition to these values,

consistent with those reported for Ag_2S, the deconvolution and fit with a single component for each doublet peak indicates the existence silver sulfide.[1]

Figure S3 shows the S 2p spectra of a sample produced in air (upper panels) and a sample produce in N_2 (lower panels). The as-prepared samples (left panels) were subject to a two-phase Ar-ion bombardment process, a methodology that allows extraction of photoelectrons at different depths from the surface. The central and right panels correspond to the samples after the first and the second ion bombardments, respectively.

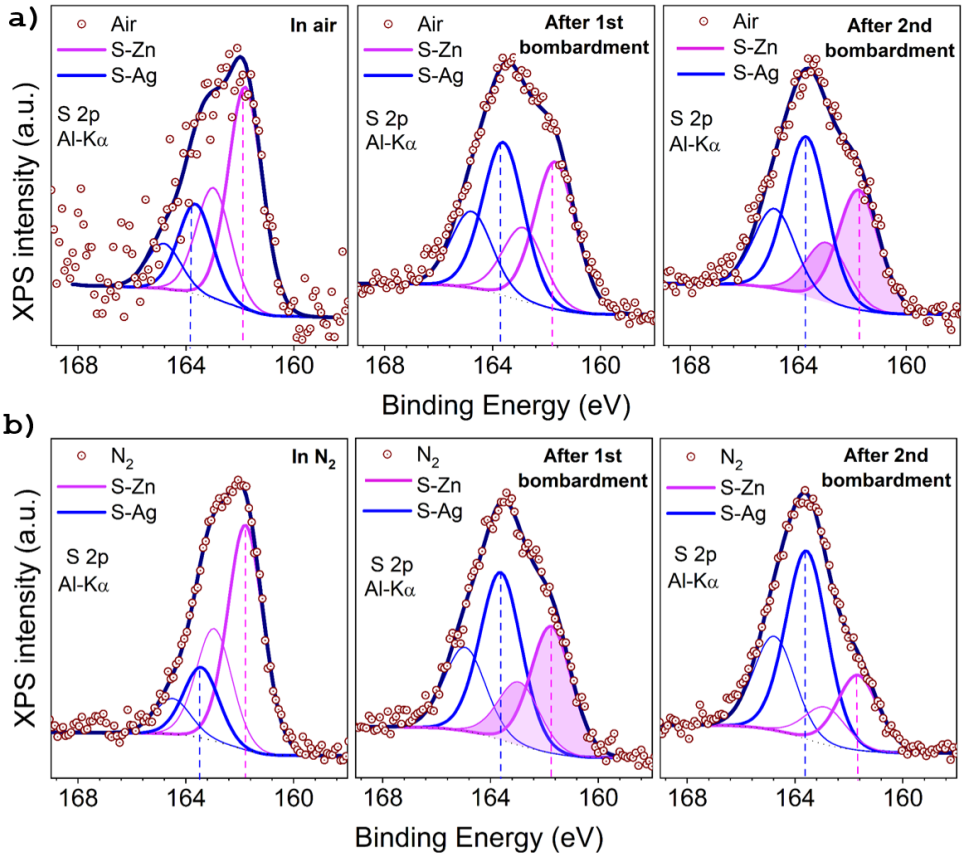

Figure S3: Upper panels: S 2p spectra of a sample produced in air before (left) and after two ion bombardment processes (middle and right panels, respectively). Lower panels: S 2p peak of a sample produced under N_2 before (left) and after two ion bombardment processes (middle and right panels, respectively). Two clear contributions related to the Zn-S (pink) and to the Ag-S (blue) are evident in all cases. It has to be noted that the Zn treatment was performed in two aliquots of the same batch of CS samples. Thus, the observed differences are exclusively related to the Zn treatment in air or N_2.

A close inspection of the S 2p spectra shows clear line-shape changes. This fact readily suggests the presence of more than a single chemical environment for S in the samples. Deconvolution and fit of the spectra cannot be done satisfactorily with a single set of two peaks corresponding to the S $2p_{3/2}$ and S $2p_{1/2}$ doublet with 1.18 ± 0.10 eV spin orbit splitting. Therefore, the addition of a second set of components is necessary, shifted by 1.8 ± 0.1 eV; this then reveals the presence of an additional chemical contribution.

XPS spectra were normalized to the maximum peak intensity in each case, for better visual inspection and direct comparison between the samples in order to highlight line-shape differences, which serves as a guide for spectra curve fitting, and contribution for each S chemical environment. Data points in every spectrum are represented as open symbols, and Shirley

background and S $2p_{3/2}$ components using solid lines (spin orbit split peaks S $2p_{1/2}$ are displayed as dotted lines). The fitting curve (dark-blue line) resulted from the addition of several contributions.

According to the evolution of the line-shape changes in the spectra upon ion bombardment, and the gradated core/shell structure of the samples, one can ascribe the component on the higher binding energy side of the spectra to S-Zn (pink). This contribution is mainly present in the as-prepared samples and decreases in intensity as ion bombardment proceeds. Conversely, the second emission at higher binding energy value corresponds to S-Ag (blue spectra), which is initially almost buried by the shell, and increases in intensity as the ion bombardment takes place and deeper regions become visible. No other peaks corresponding to higher oxidation states were detected in the S 2p core level region (sulfates are typically found at higher binding energy values of about 169 eV).

Thus, two successive ion bombardments evidence the relative decreasing of ZnS and the relative increasing of Ag_2S in both cases, in good agreement with a removal of material from the outer shell (richer in ZnS) to inner locations in the NC (richer in Ag_2S). A closer inspection to the peak areas shaded in pink show similar relative contents, both after the second bombardment for the sample produced in air and after the first bombardment for the sample produced in N_2; this suggests a thinner Zn-S shell produced under N_2.

The outcome from **Figure S3** is also evidenced in **Figure S4**, where the Zn $2p_{3/2}$ peak for the two types of samples are shown.

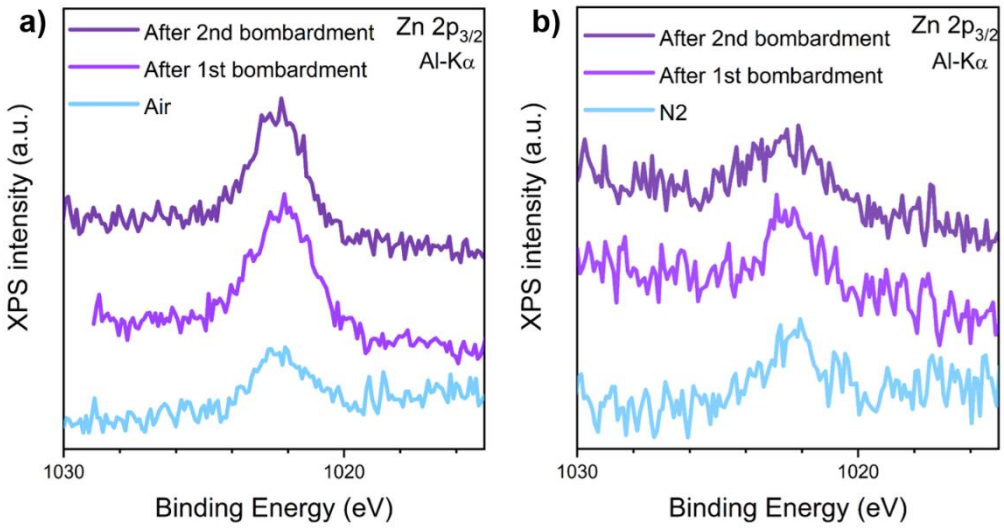

Figure S4: (a) Zn $2p_{3/2}$ peak for a CSS sample produced in air, before and after two ion bombardments. (b) Zn $2p_{3/2}$ peak for a CSS sample produced in N_2, before and after two ion bombardments.

Figures S4a and **S4b** display the evolution of the Zn $2p_{3/2}$ of the as-prepared and ion-bombarded sample produced in air and N_2, respectively. In both cases, the main peak at 1022.2 ± 0.2 eV is clearly associated to ZnS, in agreement with reported binding energy values. As both CSS samples were manipulated in air, in contact with the environment, spurious contamination and a minor presence of Zn-suboxides (no longer present after the first ion bombardment) cannot be neglected at the outermost layer of the ZnS shells.[2–6]

As shown by the comparison of the spectra of samples produced in air and N_2, the amount of Zn detected is higher in the CSS NCs synthesized in air (spectra in **Figure S4a**). In this case, an increase in the Zn signal is evident after the first ion bombardment and remains intense after the second, indicating a relatively thicker ZnS layer compared to the sample produced in N_2 (**Figure S4b**). In the latter case, after the second ion bombardment, the intensity

of the Zn $2p_{3/2}$ peak is very low (purple upper line in **Figure S4b**), suggesting that the ZnS layer is almost completely removed.

It has to be noted that photoelectrons emitted from the Zn 2p (~1022 eV) and S 2p (~161 eV) states with different binding energy values have very different kinetic energy ranges and, therefore, different probing depths. In particular, Zn 2p peaks provide surface sensitivity; their emission originates mostly from the outermost layers of the sample. In contrast, low binding energy signals from S 2p levels with higher kinetic energy are emitted from deeper regions, which significantly enhances the contribution from the core/shell as a whole, with minor influence from the outer surface layers and contaminants. Although the information provided from both core levels should be taken with care, due to the fact that Zn 2p is mainly limited to the outermost layers and due to the attenuation of S 2p signal with depth, they are fully complementary in our study.

S2.2 – Shifts in the photoluminescence (PL) response of NCs

Observation of small red and blue shifts in the PL response of NCs

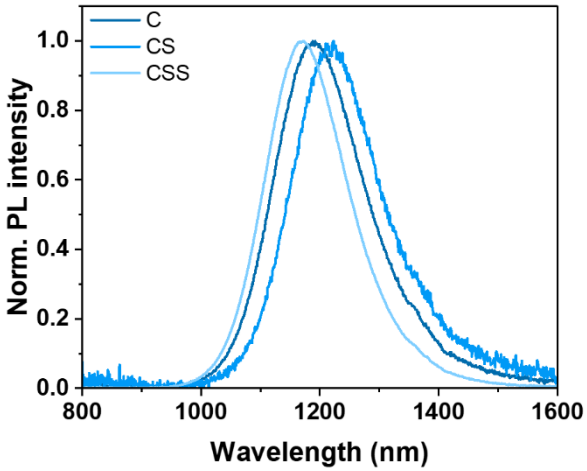

Figure S5: Normalized PL spectra of Ag_2S cores C, CS and CSS samples, evidencing a small redshift after the treatment with Se@TOP. and a small blueshift after the treatment with the Zn stock solution.

S2.3 – Transient absorption Spectroscopy – TAS

Note: All transient absorption measurements were performed with 775 nm as the excitation wavelength. The pump beam on the sample was focused to a spot size of 280 μm.

Change in ΔT/T, as a function of pump fluence

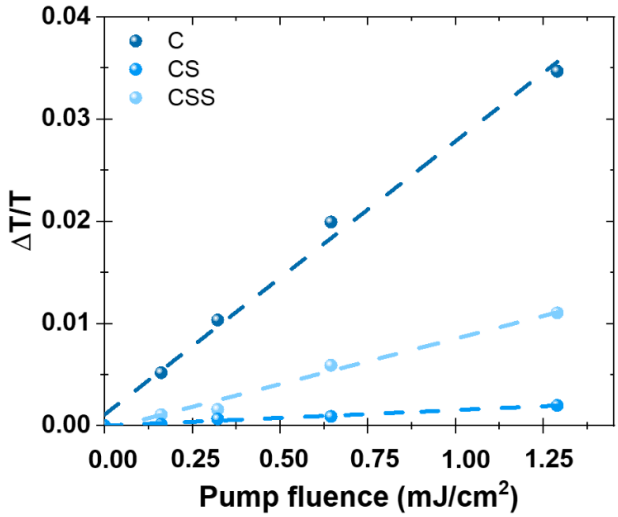

Figure S6: Maximum ΔT/T signal as a function of plump fluence for Ag_2S NCs cores (dark blue), CS (blue) and CSS (light blue).

Temporal evolution for NCs with Ag_2S and CSS cores

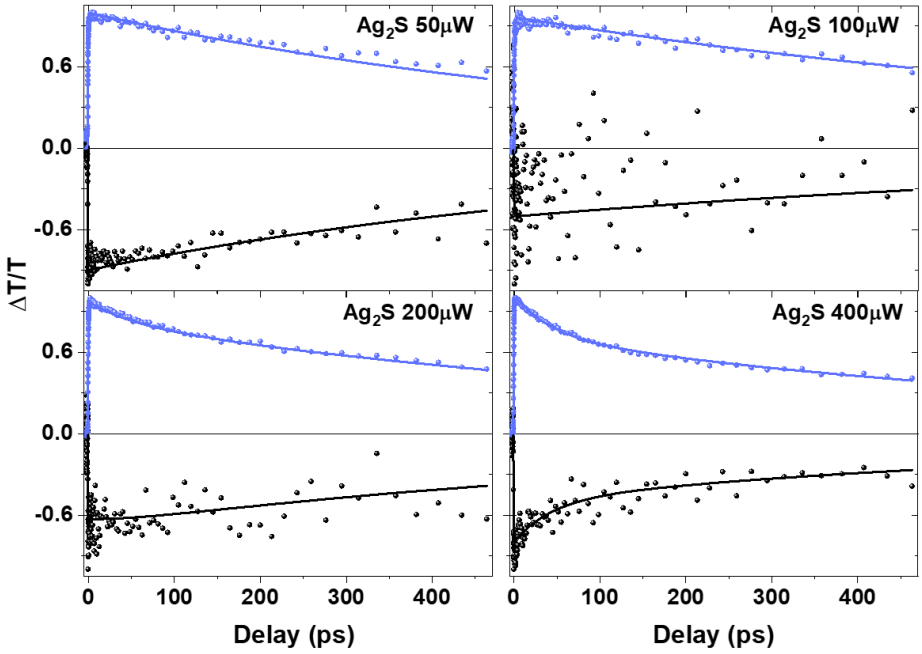

Figure S7: Temporal traces of Ag_2S NCs, for different energy fluences, at 1033 nm (blue) and 1377 nm (black). Data are represented by the dot-symbols, and fits by the lines.

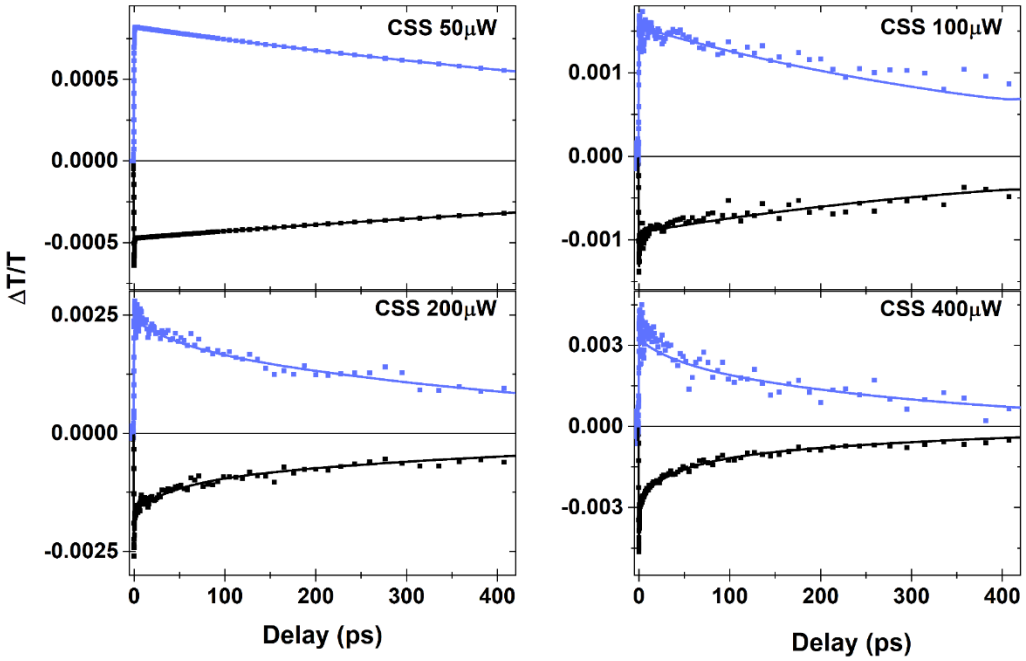

Figure S8: Temporal traces of CSS NCs, for different energy fluences, at 1033 nm (blue) and 1377 nm (black). Data are represented by the dot-symbols, and fits by the lines.

Kinetic models

The following kinetic model has been used to model TAS data, for pumping fluences of 0.16 and 0.32 mJ/cm^2:

$$\frac{dE}{dt} = G - k_1 E$$

$$\frac{dS}{dt} = k_1 E - k_2 S$$

where *E* and *S* are the initial and final states, and k_1 and k_2 are the decay rates that rule the relaxation of photoexcited states in between states.

For those measurements performed at higher fluences it was necessary to include a further relaxation process, namely Auger scattering, and the model incorporates the three rate equations:

$$\frac{dE}{dt} = G - k_1 E$$

$$\frac{dS}{dt} = k_1 E - \Gamma S^2$$

$$\frac{dF}{dt} = \Gamma S^2 - k_2 F$$

S2.4 Thermal effects

Decay dynamics with temperature

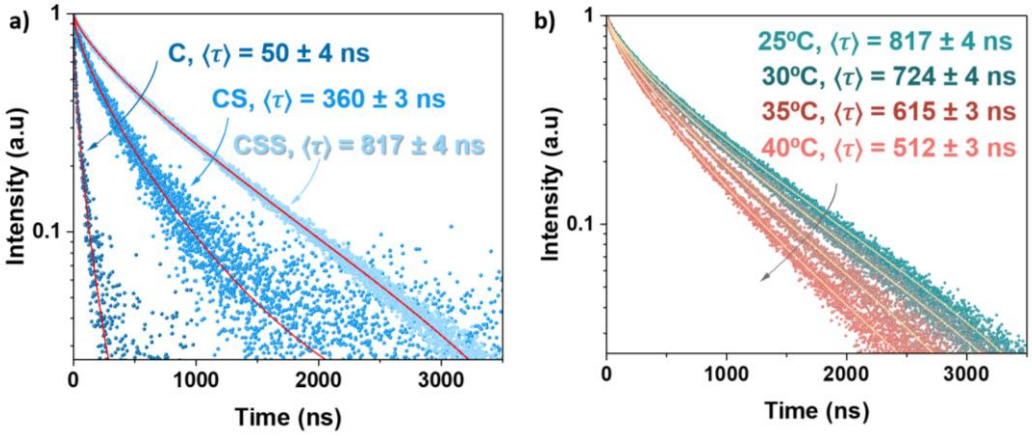

Figure S9: (a) Comparative decay dynamics for C, CS and CSS NCs samples, along with the lifetime values for each one. (b) Decay dynamics of a CSS sample in a first cycle, with increasing temperature from 25 to 40 °C, along with the lifetime for each temperature.

Thermal sensitivity experiments: Calculation of the thermal sensitivity, S

The relative thermal sensitivity is obtained by the temperature dependence of a chosen thermometric parameter, Q, being in this case the intensity ratio (integrated area) of the PL signal at 1165 nm and 1235 nm of NCs in chloroform (**Figure S10a**)) and water (**Figure S10b**)), respectively. The rationale here is that, (i) those are the wavelengths that lead to the strongest linear relationships between temperature and the ratiometric values for each data set, and (ii) parameters that present an unequivocal (linear) relationship with temperature often show a higher performance.[1] The linear fits of each data set resulted in a Pearson correlation coefficient of 0.994 in water and 0.992 in chloroform. Then, the relative sensitivity was calculated using the widely accepted equation:

$$S_R = \left|\frac{1}{Q}\frac{\partial Q}{\partial T}\right| .$$

Typically, S_R is given in units of $(\%\ ^{\circ}C^{-1})$. The derivatives were calculated from the slope of the linear calibration for each dataset. For the two data sets one finds $S_{R,CHCl3}$ = 0.34925 $^{\circ}C^{-1}$ for NCs in chloroform, and $S_{R,H2O}$ = 0.03679 $^{\circ}C^{-1}$ for NCs in water.

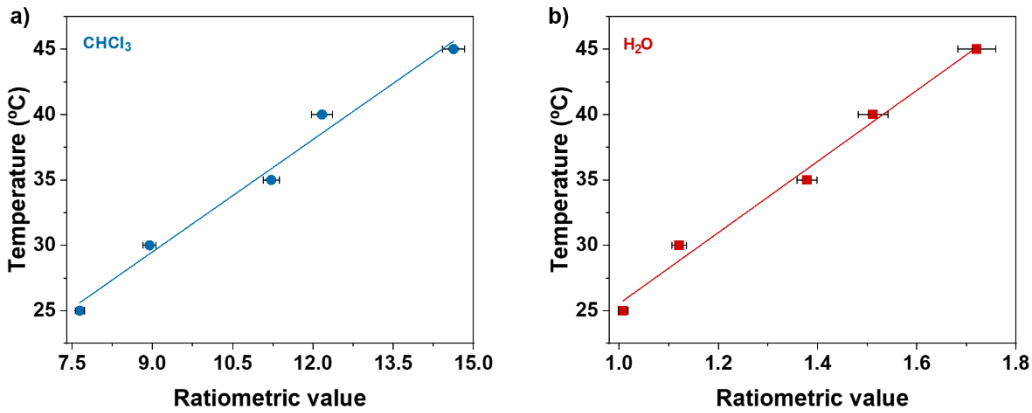

Figure S10: Temperature dependence of the ratiometric values Q, obtained as the integrated area of the PL signal (a) in chloroform and (b) in water, which are employed in determining the relative thermal sensitivity of both datasets

Behaviour of the CSS NCs in several heating/cooling cycles

Figure S11 compares three heating-cooling cycles of freshly prepared CSS NCs in water (a) and chloroform (b). The sensitive to temperature is common to both samples, since both are the same material. However, the lability of the ligands in chloroform (oleylamine) produces a loss of about 20% from the first to the second temperature cycles. In contrast, the N-PMA ligand shell used to transfer the NCs to water produces very stable NCs, very robust against temperature changes, as the PL signals basically recovers to the initial value after three consecutive cycles.

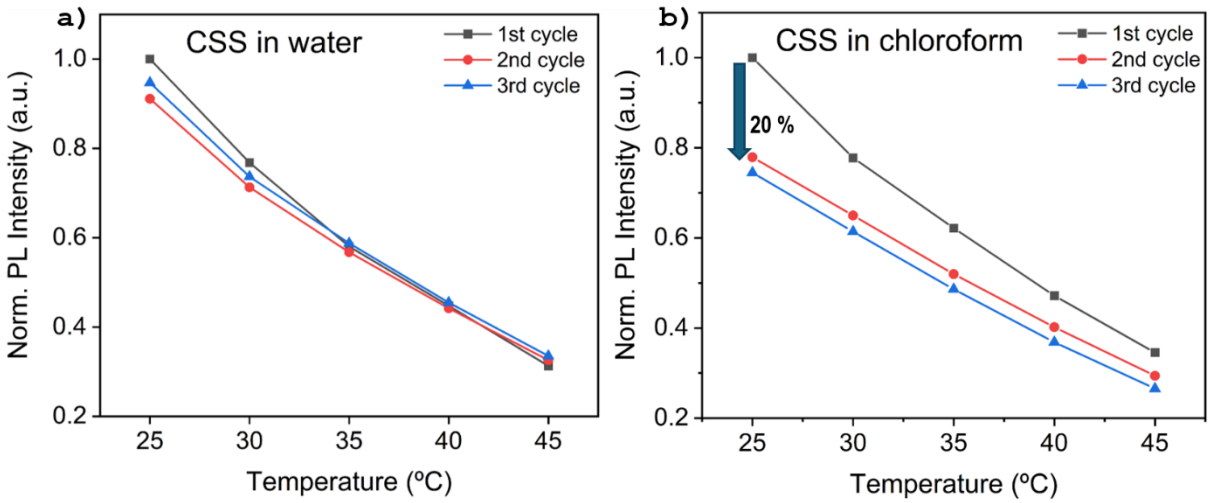

Figure S11: Comparison of the PL response with temperature of (a) CSS NCs in water and (b) in chloroform after three consecutive heating-cooling cycles.

S2.5 Extinction of CSS in chloroform and water: a comparison

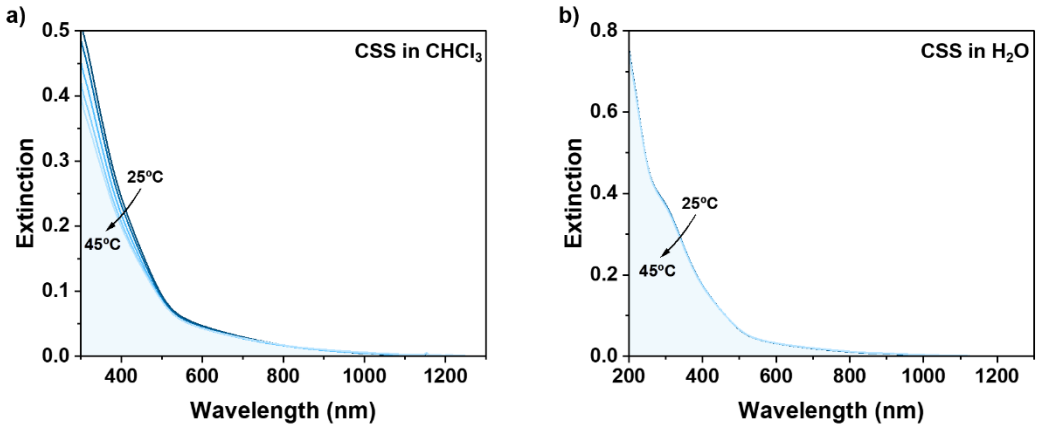

Figure S12: Extinction of CSS NCs in chloroform (a) and in water (b) with temperature, where minor changes can be observed in both cases

References

1 D. G. Calatayud, T. Jardiel, M. Peiteado, F. Illas, E. Giamello, F. J. Palomares, D. Fernández-Hevia and A. C. Caballero, *J Phys Chem C*, 2015, **119**, 21243–21250.

2 Zinc (Zn), Z=30, & Zinc Compounds, https://xpsdatabase.net/zinc-zn-z30-chemicals/, (accessed July 31, 2024).

3 D. Barreca, A. Gasparotto, C. Maragno, E. Tondello and T. R. Spalding, *Surf Sci Spectra*, 2003, **9**, 54–61.

4 N. Dengo, A. Vittadini, M. M. Natile and S. Gross, *J Phys Chem C*, 2020, **124**, 7777–7789.

5 A. Arulraj, N. Ilayaraja, V. Rajeshkumar and M. Ramesh, *Sci Rep*, 2019, **9**, 10108.

6 Z. Tang, H. Yang, Z. Sun, Y. Zhang, G. Chen and Q. Wang, *Nano Res*, 2023, **16**, 12315–12322.